# Resolving heterogeneous dynamics of excess protons in aqueous solution with rate theory

Santanu Roy,\*,† Gregory K. Schenter,‡ Joseph A. Napoli,¶ Marcel D. Baer,‡

Thomas E. Markland,¶ and Christopher J. Mundy\*,‡,§

† Chemical Sciences Division, Oak Ridge National Laboratory, 1 Bethel Valley Rd., Oak Ridge, TN 37830, USA

‡Physical Sciences Division, Pacific Northwest National Laboratory, 902 Battelle Blvd,
Richland, WA 99352, USA

¶Department of Chemistry, Stanford University, 333 Campus Drive Stanford, CA 94305,

USA

§Affiliate Professor, Department of Chemical Engineering, University of Washington, Seattle, USA

E-mail: roys@ornl.gov; chris.mundy@pnnl.gov

#### Abstract

Rate theories have found great utility across the chemical sciences by providing a physically transparent way to analyze dynamical processes. Here we demonstrate the benefits of using transition state theory and Marcus theory to study the rate of proton transfer in HCl solutions. By using long *ab initio* molecular dynamics simulations we show that good agreement is obtained between these two different formulations of rate theory and how they can be used to study the pathways and life-time of proton transfer in aqueous solution. Since both rate theory formulations utilize identical sets of molecular data, this provides a self-consistent theoretical picture of the rates of

aqueous phase proton transfer. Specifically, we isolate and quantify the rates of proton transfer, ion-pair dissociation, and solvent exchange in concentrated HCl solutions. Our analysis predicts a concentration dependence to both proton transfer and ion-pairing. Moreover, our estimate of the life-time for the Zundel species is 0.8 ps and 1.3 ps for 2M and 8M HCl, respectively. We demonstrate that concentration effects, can indeed be quantified through the combination of state-of-the-art simulation and theory and provides a picture of the important correlations between the cation (hydronium) and the counter-ion in acid solutions.

#### Introduction

Discovering and quantifying the pathways and rates of proton transport and understanding its multidimensional behavior to control proton conduction continues to be the central focus of various modern energy technologies. <sup>1-4</sup> While the structures of small protonated gas phase water clusters have been well established using both experiment <sup>5-7</sup> and theory <sup>8,9</sup> the structures formed by aqueous proton defects in the condensed phase and the mechanism of their interconversion still provokes significant debate. For the case of the isolated reactive proton defect, there have been numerous high-quality studies using reactive force fields that yield a consistent picture of the *intrinsic* free-energy landscape of the isolated hydrated proton. <sup>10-21</sup> The speciation of the hydrated proton to the air-water interface is still an active area of research requiring the use of difficult to interpret surface-sensitive spectroscopy in addition to large-scale simulation using reactive force-fields. <sup>10-13,15-26</sup> Moreover, the consistency of simulation studies with the well accepted surface tension measurement of acids remains uncertain. <sup>27,28</sup> This requires an understanding of the correlation between the proton (*e.g.* cation) with the counter ion in concentrated acid solutions. <sup>29-33</sup>

To understand the role of counterions in acid solutions, pioneering x-ray measurements have been undertaken to understand ion-pairing in concentrated acids under bulk homogeneous conditions.<sup>29–31</sup> These studies have provided insights into the transition, as the

acid concentration is increased, from fully dissociated acids to associated (molecular or ionpaired). <sup>29,30</sup> Moreover, extended x-ray absorption fine structure (EXAFS) measurements of HCl detected a new correlated species, a contracted contact ion-pair, that exists between the hydrated proton and the chloride ion over a wide range of concentrations.<sup>31</sup> This measurement suggests that when examining the structure and dynamics of the hydrated proton in aqueous solution, the counterion cannot be treated as a spectator. This realization has possible implications for viewing the proton in analogy to a (monovalent) cation in an inorganic salt (e.g. electrolyte) where ion-ion correlation for monovalent salts can be neglected at low ionic strength. 34,35 Pioneering 2D infrared (2D IR) experiments have deduced the life-time of the hydrated Zundel complex in 4M HCl by probing the characteristic stretch and bend modes in the first hydration shell of the proton defect.<sup>32</sup> This novel prediction of a lower bound on the life-time of a "Zundel" like species (480 fs<sup>32</sup>) inspired simulation studies in an attempt to provide a molecular picture of the findings. 19,36,37 Napoli et. al. 37 produced long trajectories using quantum density functional theory (DFT) based interaction potentials (with both quantum and classical nuclei) of both 2M and 4M HCl solutions. Using these simulations they were able to demonstrate the importance of a asymmetry coordinate that distinguishes the hydrogen bonding asymmetry of the solvating acceptor water molecules around the proton defect. This work demonstrated that the relaxation timescale of this asymmetry coordinated was in good agreement with the estimates of the "Zundel" life-time measured by 2D IR. 32 This suggests that what was being experimentally probed was related to the collective reorganization of the hydrogen bond network about the proton defect and that this is correlated to the life-time of the Zundel like complexes formed in the liquid.<sup>37</sup> More recently the hopping rate of protons in water was directly determined experimentally by monitoring 2D IR chemical exchange using a methyl thiocyanate vibrational probe.<sup>38</sup>

In the present work we use the framework of rate theory <sup>39–53</sup> to separate the contributions to the dynamics of different molecular phenomena, such as ion-pairing and solvent exchange, that occur in concert with proton transfer. In the standard application of rate theory to ion-

pairing one can employ a simple interionic distance as the reaction coordinate to investigate ion-pairing and solvent exchange events.  $^{54-65}$  According to transition state theory (TST), when the system arrives at the transition state (the top of the free energy barrier) from the reactant state, it immediately traverses to the product state. This assumption generally does not work using distance between reacting species as a reaction coordinate because of the strong coupling to the fluctuating solvent bath leading to significant barrier-recrossing. The non-equilibrium solvent effect is quantified, by multiplying the TST rate with a transmission coefficient,  $\kappa$ , as shown in Equation 1.  $^{45,47-49,66,67}\kappa$  can be formulated in terms of the fraction of the flux of reacting trajectories through dividing surface that produces the desired product state and a small value is indicative of an inferior reaction coordinate.

$$k_{\text{TST}}^{\text{Correct}} = \frac{\kappa}{\sqrt{2\pi\mu\beta}} \frac{q^{\dagger 2} \exp\left[-\beta W(q^{\dagger})\right]}{\int_{0}^{q^{\dagger}} q^{2} \exp\left[-\beta W(q)\right] dq}.$$
 (1)

Here  $\mu$  is the reduced mass for the dynamics along the reaction coordinate, q. W(q) is the free energy profile, wherein  $q^{\dagger}$  is the location of the transition state, and  $\beta=1/k_{\rm B}T$  is the inverse of thermal energy where  $k_{\rm B}$  and T are the Boltzmann constant and temperature, respectively. In Equation 1, we considered the spherically symmetric nature of the reaction coordinate, q, that leads to the  $q^2$  Jacobian term. The more general expressions will be employed later in the manuscript. In TST,  $\kappa$  is assumed to be unity. However, strong non-equilibrium solvent effects can lead to  $\kappa \ll 1$ , providing significantly deviations from TST rates. <sup>54–64</sup>

To improve upon the standard TST formulation given in Equation 1, a direct incorporation of solvent fluctuations as an additional reaction coordinate for describing the phenomena of ion-pair dissociation and solvent exchange has been recently formulated by Roy and coworkers. <sup>68–70</sup> This additional complexity in defining the reaction coordinate will allow us to compare and contrast two different approaches for investigating rate processes in condensed phase systems. First, the standard formulation of rate theory (as stated above) in conjunc-

tion with reactive flux calculations will yield a time-dependent transmission coefficient for the reaction coordinate outlined herein, revealing the temporal behavior of thermal energy transfer from the coupling between the solvent to the reaction coordinate. 71 Second, as we have demonstrated in our previous studies, <sup>68–70</sup> the (2D) representation of the reaction coordinate that incorporates both distance and solvent fluctuations can be mapped to an efficient one-dimensional Marcus-like theory. While fluctuations in both coordination number and electric field can be utilized to examine solvent fluctuations, <sup>68–70</sup> we consider electric field to represent solvent fluctuations. This is because, fluctuating coordination number may lack information about the solvent rearrangement beyond the first and second shells, whereas the electric field that a solute molecule experiences includes the effects of solvent rearrangement from the entire solvent. Furthermore, electric field has been proven to be an excellent collective variable to examine solvent effects in vibrational spectroscopy and has been used in modeling spectroscopic observables such as transition frequencies, dipole moments, and polarizability. $^{72-74}$  Thus, by exploring both distance and electric field within the framework of TST and Marcus theory we wish to provide a clear, in-depth, self-consistent physical picture regarding the effects of ion-pair dissociation and solvent exchange on the kinetics and pathways of proton transfer.

### Theory and Simulation

#### Two-dimensional transition state theory

To formulate TST for a system described by the intrinsic reaction coordinate,  $R_c = (q, E(q))$  with q being the interionic/molecular distance and E being the solvent-exerted electric field on the solute projected along a particular direction (see Results and Discussion for specific cases), and the rest of the degrees of freedom as the solvent bath coordinate (B), we first make a coordination transformation from a set of Cartesian coordinates X of 3N components (N) is the number molecules including ions) to the set of  $(R_c, B)$ , where B has 3N - 2

components. The conjugate momenta associated with this new set are  $p_q$ ,  $p_E$ , and  $P_B$  with 3N-2 components, which are transformed from the Cartesian momentum  $P_X$  with 3N components. We adopt the formalism of constructing a multi-dimensional Hamiltonian in generalized coordinate space.<sup>75</sup> Here the Hamiltonian can be straightforwardly expressed as:

$$H = \frac{1}{2}Z_{q}p_{q}^{2} + \frac{1}{2}Z_{E}p_{E}^{2} + Z_{qE}p_{q}p_{E} + \frac{1}{2}P_{B}^{T}Z_{B}P_{B} + V(q, E, B)$$

$$= K(q) + K(E) + K(q, E) + K(B) + V(q, E, B). \tag{2}$$

The first four terms in Equation 2 are the kinetic energy terms (the cross-terms between  $p_q$  and  $P_B$  and between  $p_E$  and  $P_B$  have been ignored) and the last one is the potential energy. For a generalized coordinate,  $\xi=q$  or  $\xi=E,\ Z_{\xi}=\sum_{i=1}^{i=3N}\frac{1}{m_k}\left(\frac{\partial \xi}{\partial x_k}\right)^2$ , where  $m_k$  is the mass associated with the  $k^{\text{th}}$  component  $(x_k)$  of the Cartesian coordinate, X. Likewise,  $Z_{qE} = \sum_{i=1}^{i=3N} \frac{1}{m_k} \left( \frac{\partial q}{\partial x_k} \right) \left( \frac{\partial E}{\partial x_k} \right)$ . In the case of water exchange around hydronium or dissociation of hydronium chloride,  $Z_q$  is associated with the oxygen-oxygen or oxygenchlorine reduced mass,  $\mu$ :  $Z_q = 1/\mu = \left(\frac{1}{m_{\rm O}} + \frac{1}{m_{\rm O/Cl}}\right)$ , where  $m_{\rm O}$  and  $m_{\rm Cl}$  are the mass of oxygen and chlorine, respectively. For the proton transfer we consider that the donor oxygen-proton-acceptor oxygen angle is 180°; therefore,  $Z_q = \left(\frac{2}{m_{\rm O}} + \frac{4}{m_{\rm H}}\right)$ . 43 To determine  $Z_E$ , we consider the electric field on a solute ion or atom exerted by the remaining solution along a chosen direction,  $\hat{e}$ :  $E = \hat{e} \cdot \sum_{i=1}^{N-1} \frac{Q_i}{r_i^2} \hat{r_i}$ , where  $Q_i$  is the partial charge of the  $i^{\text{th}}$ atom/ion exerting electric field from a distance  $r_i$  in the  $\hat{r_i}$  direction. We utilize the Dang-Chang model<sup>59,76</sup> to assign partial charges to H and O atoms of hydronium and water, while -1 was assigned to Cl<sup>-</sup>. In analogy with our formulation of rate theory using coordination number as a coordinate  $^{68,77}$  the expression for  $Z_E$  associated with the E-space dynamics takes the form,

$$Z_E = \sum_{i}^{N-1} \frac{f_i'^2}{\mu_i} + \frac{2}{M} \sum_{i=1}^{N-2} \sum_{j=i+1}^{N-1} f_i' f_j' \frac{\vec{r_i} \cdot \vec{r_j}}{|\vec{r_i}||\vec{r_j}|}.$$
 (3)

Here  $f'_i$  is the derivative of the electric fields  $(E_i)$  on an atom of interest with the mass, M, exerted by  $i^{\text{th}}$  atom located at a distance  $r_i$ , i.e.,  $f'_i = \left(\frac{\partial E_i}{\partial r_i}\right) = -\frac{2Q_i}{r_i^3}(\hat{e} \cdot \hat{r}_i)$ .  $f'_j$  describes the same as  $f'_i$ , but due to the  $j^{\text{th}}$  atom.  $\mu_i$  is the reduced mass of the  $i^{\text{th}}$  atom and the atom experiencing the electric field. Likewise,  $^{68}$   $Z_{qE}$ , which is associated with the correlated motion between q and E, can be expressed as:

$$Z_{qE} = \sum_{i}^{N-1} f_{i}' \frac{\vec{r_{i}} \cdot \vec{q}}{|\vec{r_{i}}||\vec{q}|}.$$
 (4)

Given knowledge of the Hamiltonian shown in Eq. 2, the joint probability distribution, P(q, n), can be determined through integration over the variable q' and E':<sup>75</sup>

$$P(q, E) = \frac{1}{C} \int dX dP_X \delta(q' - q) \delta(E' - E) \exp(-\beta H), \tag{5}$$

where C is the normalization constant and dX and  $dP_X$  are the phase space variables (which, as aforementioned, can be transformed to the reaction coordinate variables, q' and E', and the bath variable B). Equation 5 utilizes the property of the delta functions: The integral vanishes unless q' = q and E' = E, providing ensemble-averaged joint probability of finding q' = q and E' = E. By exploring all possible values of q and E, the joint probability distribution for these coordinates can be obtained in the entire joint space of q and E. The 2D PMF, W(q, E), is related to P(q, E) via:

$$W(q, E) = -k_{\rm B}T \ln P(q, E) + 2k_{\rm B}T \ln(q) + W'.$$
(6)

Here, W' is a constant introduced to shift the global minimum of W(q, E) to zero. In practice, we obtain W(q, E) from our DFT simulations by computing a 2D-histogram of q and E: If there are dN number of cases where distance is between q and q + dq and the electric field is between E and E + dE, then W(q, E) is expressed as  $W(q, E) = -k_{\rm B}T \ln(dN/4\pi q^2 dq dE \rho)$  where  $4\pi q^2 dq dE$  is the volume element of the joint q - E space and  $\rho$  is the number density

(number of atoms/molecules/ions per unit volume). This straightforwardly resembles Eq. 6, in addition to constants such as logarithms of  $\rho$ , dE, and dq that are included in W'.

The general expression for the TST rate for a dividing surface described by the parametric equation, S(X) = 0, is given by:

$$k_{\text{TST}}^{2D} = \frac{1}{Q_{\text{R}}} \int dX dP_X \Theta(\dot{S}) \dot{S} \delta(S) \exp[-\beta H], \tag{7}$$

where,  $\dot{S} = \frac{\partial S}{\partial X} \frac{d}{dt} X$ , is the time derivative of S.  $\Theta(\dot{S})$  selects trajectories in phase space that are initially heading towards products.  $Q_{\rm R} = \int_{\rm R} dX dP_X \exp[-\beta H]$  is the reactant partition function ( $\int_{\rm R}$  indicates integral over only the reactant region R). Thus, we find

$$Q_{\rm R}k^{\rm TST} = \text{Tr}\left[e^{-\beta H}\delta\left(q\right)\frac{d}{dt}q\,\theta\left(\frac{d}{dt}q\right)\right],$$
 (8)

where we assume that the dividing surface, S(q) = 0, only depends on the interionic distance, q. Equation 8 further provides

$$Q_{\rm R}k^{\rm TST} = \frac{e^{-\beta W^{\dagger}}}{2\pi\sqrt{K_E \left(Z_E - Z_{qE}^2/Z_q\right)}}$$

$$\tag{9}$$

$$W\left(q^{\dagger}, E\right) = W^{\dagger} + \frac{1}{2}K_{E}E^{2} \tag{10}$$

We employed the reactive flux method <sup>49</sup> to determine the transmission coefficient-corrected TST timescales ( $\tau = 1/\kappa_{RF}k_{TST}$ ). The reactive flux transmission coefficient is a time-dependent quantity defined by,

$$\kappa_{\rm RF}(t) = \frac{\langle v_q(0)\Theta[q(t) - q^{\dagger}]\delta(q(0) - q^{\dagger})\rangle}{\langle v_q(0)\Theta[v_q(0)]\delta(q(0) - q^{\dagger})},\tag{11}$$

where q(0) and  $v_q(0)$  are respectively the initial value of q and associated velocity at the top of the barrier  $(q^{\dagger})$  on the W(q), and  $\Theta$  is a Heaviside step function.

#### Marcus theory

Marcus theory of ion-pairing and solvent exchange allows us extract the reactant and product states from the 2D PMF as the parabolic functions of electric field. In this theory, the reactant,  $W(q_R, E)$ , and the product,  $W(q_P, E)$ , free energies can be expressed as:

$$W(q_{\rm R}, E) = W_{\rm R}(E) = \frac{1}{2}K_{\rm R}E^2$$
  
 $W(q_{\rm P}, E) = W_{\rm P}(E) = \frac{1}{2}K_{\rm P}(E - E_{\rm P})^2 + \Delta W,$  (12)

where  $K_{\rm R}$  and  $K_{\rm P}$  are the curvatures of the reactant and product parabolas with the minima, E=0 and  $E=E_{\rm P}$ , respectively.  $\Delta W=W_{\rm P}(E_{\rm P})-W_{\rm R}(0)$ , is the free energy difference between the product and reactant equilibria. Marcus parabolas are diabatic states that cross at a point through which the transitions between the reactant and product states occur driven by solvent rearrangement. The free energy barrier corresponding to this transition state,  $\Delta W^{\dagger}$ , can be determined straightforwardly (Eq. 13) by considering  $K_{\rm R}=K_{\rm P}$ .  $\Delta W^{\dagger}$  is related to the free energy difference between the reactant and product,  $\Delta W$ , and the solvent reorganization energy,  $\lambda$ , the energy cost required for transforming the equilibrium reactant coordination number to the equilibrium product coordination number, *i.e.*,  $\lambda=W_{\rm R}(E_{\rm P})-W_{\rm R}(0)$ .

$$\Delta W^{\dagger} = \frac{(\lambda + \Delta W)^2}{4\lambda}.\tag{13}$$

However, the free energy barrier can be sensitive to the difference between the curvatures of reactant and product parabolas as discussed in our earlier study.<sup>69</sup> The curvature difference leads to a couple of crossing points, but the reactant-to-product transition should occur most-likely through the one with the lowest barrier as given below:<sup>69</sup>

$$\Delta W^{\dagger} = \frac{K_{\rm P}(K_{\rm R} + K_{\rm P})}{\Delta K^2} \lambda + \frac{K_{\rm R}}{\Delta K} \Delta W - \frac{\sqrt{2}E_{\rm P}K_{\rm R}K_{\rm P}}{\Delta K^2} \sqrt{[K_{\rm P}\lambda + \Delta K\Delta W]}. \tag{14}$$

Analogous to Wigner's TST, then the transition rate can be determined by the following expression: <sup>68,78</sup>

$$k_{\text{Marcus}} = \frac{k_{\text{B}}T}{h} \exp[-\Delta W^{\dagger}/k_{\text{B}}T].$$
 (15)

It is worth to note that we have chosen the prefactor,  $\frac{k_{\rm B}T}{h}$ , for simplicity, assuming that it will not affect significantly and provide similar rates when compared to a more accurate prefactor specific to electric field. However, if one may require, we recommend to explore the formalism presented in our previous work<sup>43,77</sup> for determining accurate prefactors for specific reaction coordinates.

In the exact formulation of Marcus theory the ion-pair dissociates spontaneously leading to the product state as soon as the crossing point between the reactant and product parabolas is reached. Importantly, the fluctuations of the surrounding solvent that couples to the motion along the reaction coordination can lead to barrier-recrossing, which can effectively reduce the number of barrier crossings. The semi-classical approach of Landau<sup>79,80</sup> and Zener<sup>81</sup> can be adopted to account for such solvent effect through the determination of the associated transmission coefficient ( $\kappa_{LZ}$ ).  $\kappa_{LZ}$  depends on the probability (P) of the reactive transitions through the crossing region as well as the location of the crossing region: <sup>68,82</sup>

$$\kappa_{\rm LZ} = \begin{cases}
2P/(P+1) & \text{at "normal region"} \\
2P(1-P) & \text{at "abnormal region"}.
\end{cases}$$
(16)

The "normal region" and "abnormal region" denote a curve crossing region at the opposite and same sides of the parabolas, respectively. P is related to the coupling (C) between the reactant and product parabolas and the positive traversal velocity  $(v_E)$  in electric field space at the crossing point:

$$P = 1 - \exp\left[-\frac{2\pi C^2}{\hbar v_E |S_2 - S_1|}\right],\tag{17}$$

where  $S_{1,2} = \frac{dW(E)}{dE}|_{E=E^{\dagger}}$  are the slopes of the parabolas at the crossing point and  $v_E$  is the mean value of the traversal velocity distribution, D(v), at the crossing point obtained from the phase space trajectories of electric field. D(v) has an exponential form:  $D(v) = D_0 \exp(-v^2/\sigma^2)$ , and thereby  $v_E$  can be obtained as  $v_E = \int vD(v)dv$ . Assuming that the curvature of the reactant and product parabolas are unequal, the coupling C at the crossing point  $(E=E^{\dagger})$  takes the form of;  $C(E) = \frac{K_R + K_P}{2\sqrt{K_R K_P}} \sqrt{\left[W_R(E) - W_R(0)\right] \left[W_P(E) - W_P(E_p)\right]}$ , where the prefactor disappears for  $K_R = K_P$ . <sup>68</sup> The probability of reactive transition, therefore  $\kappa_{LZ}$ , is dominated by the reactant-product coupling strength, C, essentially affecting the transition rates. After incorporating  $\Delta W_r^{E^{\dagger}}$  and  $\kappa_{LZ}$ , the corrected Marcus rate expression becomes:

$$k_{\text{Correct}}^{\text{Marcus}} = \kappa_{\text{LZ}} k_{\text{Marcus}} \exp\left[-\Delta W_r^{E^{\dagger}}/k_{\text{B}}T\right].$$
 (18)

#### Ab initio molecular dynamics simulations

We performed classical *ab initio* molecular dynamics simulations of concentrated hydrochloric (HCl) acid solutions in the NVT ensemble at T=300 K under periodic boundary conditions. The potential energy surface was represented using the GGA level of density functional theory (DFT). 2M and 8M HCl solutions were simulated at their experimental densities.<sup>83</sup>

Dynamics were generated using the i-PI program<sup>84,85</sup> and employed a multiple timescale (MTS) integrator of the r-RESPA form.<sup>86</sup> All simulations employed a 2.0 fs outer time step for integrating the full forces and a 0.5 fs inner time step for integrating the reference forces. Initial configurations for the DFT simulations were obtained according to a multi-step procedure detailed previously.<sup>37</sup> 5 ps equilibration runs were performed for each trajectory using a local Langevin thermostat with a time constant of 25 fs, while production runs used a global stochastic velocity re-scaling (SVR) thermostat<sup>87</sup> with a time constant of 1 ps. The global coupling of the SVR thermostat results in negligible perturbation to the dynamics of the systems.<sup>88</sup> In aggregate, we performed 555 ps and 400 ps of 2M HCl and 8M HCl,

respectively.

Full forces were evaluated at the DFT level of electronic structure theory using the CP2K program  $^{89,90}$  and the revPBE  $^{91,92}$  GGA functional, with D3 dispersion corrections  $^{93}$  added. Atomic cores were represented using the dual-space Goedecker-Tetter-Hutter pseudopotentials.  $^{94}$  Within the GPW method,  $^{95}$  Kohn-Sham orbitals were expanded in the TZV2P basis set, while an auxiliary plane-wave basis with a cutoff of 400 Ry was used to represent the density. The self-consistent field cycle was converged to an electronic gradient tolerance of  $\epsilon_{\rm SCF} = 5 \times 10^{-7}$  using the orbital transformation method,  $^{96}$  with the initial guess provided by the always-stable predictor-corrector extrapolation method  $^{97,98}$  at each time step. The MTS reference forces were evaluated at the SCC-DFTB3  $^{99}$  level of theory using the DFTB+ program.  $^{100}$  The 3ob parameter set was used to describe the H and O atoms,  $^{101}$  and was combined with a parameterization for hydrated halide ions.  $^{102}$  Dispersion forces were included via a Lennard-Jones potential,  $^{103}$  whose parameters were taken from the Universal Force Field.  $^{104}$ 

#### Results and Discussion

In order to accurately employ either TST or Marcus theory utilizing a 2D reaction coordinate  $R_c$  for the problem, it is necessary that the reactant and the product states are clearly distinguishable on the 2D-free energy surface. For the case of a concentrated HCl solution relevant to this study, this is clearly demonstrated in Figure 1. In Figure 1a, we consider the 2D reaction coordinate,  $R_c(q, E)$ . Here q represents the distance between a hydronium oxygen and a chloride ion and between a hydronium oxygen and a water oxygen in the study of ion-pair dissociation and water exchange, respectively. The electric field, E is exerted by the solvent bath and calculated on the chloride ion or the water oxygen and projected along the direction from the hydronium oxygen to the chloride ion or the water oxygen. For investigating proton transfer, we use the standard difference coordinate, namely the distance

between the donor oxygen-proton distance  $(q_1)$  and the acceptor oxygen-proton distance  $(q_2)$ :  $q = q_1 - q_2 - q_0 = \delta q - q_0$ , where  $q_0$  is a constant. Here, the electric field is calculated on the whole donor water-proton-acceptor water fragment and projected along the direction from the donor oxygen to the proton. The concomitant 2D-free energy landscape determined from the populations harvested using our DFT simulations (described in detail below) and the descriptor defined in Figure 1a result in W(q, E) where all three cases are well-resolved, namely proton transfer, ion-pair dissociation, and solvent exchange. By performing wavelet transform of the proton transfer coordinate, we obtain Figure 1b wherein we indeed find that the "Zundel" like state is frequency-resolved (1000-1500 cm<sup>-1</sup>) and is red-shifted from the "Eigen" like structure ( $\sim$ 2500 cm<sup>-1</sup>). Having established the imperative of possessing a free-energy with distinct extrema, we proceed to utilizing the tools of rate theory to determine how the underlying solution conditions, namely HCl concentration, control the dynamics and pathways of proton transfer in aqueous solution.

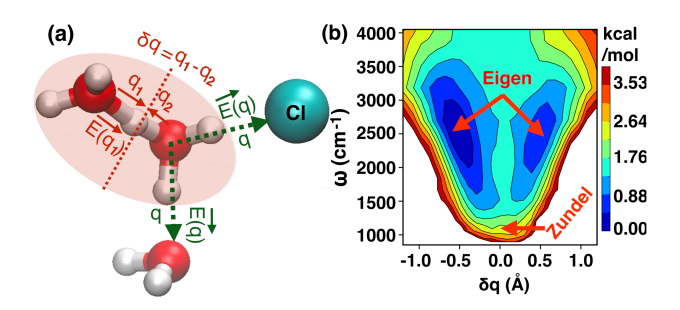


Figure 1: 2D-reaction coordinate,  $R_c$ , describing proton shuttles between two water molecules  $(R_c = (\delta q, E(q_1)))$  and vehicular motion of protons carried by  $H_3O^+$  through  $H_3O^+$ -Cl<sup>-</sup> and  $H_3O^+$ -H<sub>2</sub>O dissociations  $(R_c = (q, E(q)))$  (a). The 2D-free energy,  $W(\delta q, \omega)$ , indicates that the Eigen hydronium and Zundel states are frequency-resolved; as the proton moves away from the Eigen states (free energy minima) towards the Zundel state (free energy barrier plateau), its frequency gets red-shifted (b).

There are two competing mechanisms that describe proton transport in aqueous solution:i) a proton either shuttles between two water molecules, ii) or gets carried by a water molecule in the form of hydronium exhibiting vehicular motion. Our focus here is to dynamically quantify and separate both of these processes using rate theory. By exploring PMFs in the distance and electric field space we discuss the shuttling motion in Figure 2. In Figure

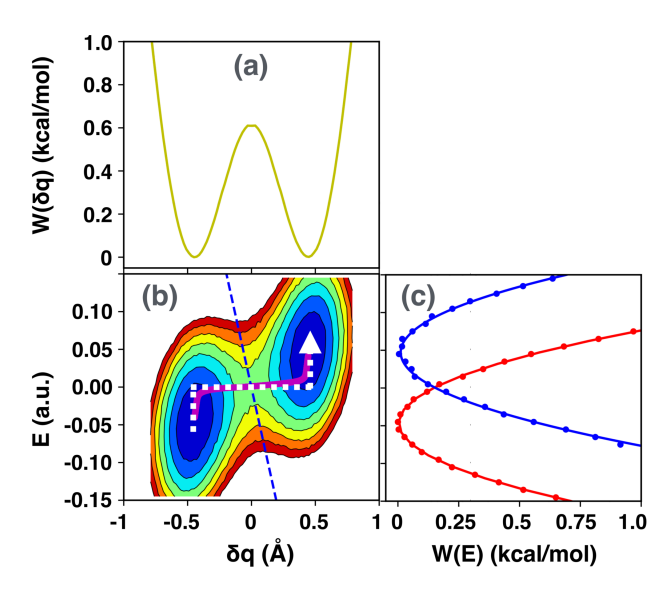


Figure 2: The 1D PMFs,  $W(\delta q)$  (a) and W(E) (c) and the 2D PMF,  $W(\delta q, E)$  (b) describing that minimum free energy pathway (white, dashed) and Marcus pathway (red, solid) of proton transfer are in excellent agreement. Blue, dashed line indicate dividing surface perpendicular to the minimum free energy pathway. Dotted lines in W(E) are slices (dotted line) from  $W(\delta q, E)$  representing the reactant,  $W_R(E)$  and the product,  $W_R(E)$ , that are fitted with parabolas (solid line). In  $W(\delta q, E)$ , 8 contours are evenly placed between 0 kcal/mol and 1.2 kcal/mol.

3 we present two distinct pathways for vehicular motion. First, a pathway associated with the dissociation of the ion-pair, H<sub>3</sub>O<sup>+</sup>-Cl<sup>-</sup>, and the second corresponding to water exchange around hydronium that requires breaking and reforming of H<sub>3</sub>O-H<sub>2</sub>O hydrogen bonds. In Figure 2 and Figure 3, we consider these pathways only for 8M HCl, while in the Supporting Information (SI) (Figures S1, S2, and S3) we provide a comparison between the effects of ionic strengths (namely, 2M and 8M HCl) on them.

The PMF in Figure 2,  $W(\delta q)$ , is obtained by integrating  $W(\delta q, E)$  over the entire electric field space, i.e.  $\exp[-\beta W(\delta q)] = \int dE \exp[-\beta W(\delta q, E)]$ , and allows us to pinpoint the equilibrium location of the proton at the reactant  $(\delta q = -0.45 \text{ Å})$  and product hydronium state  $(\delta q = 0.45 \text{ Å})$ . The slices of  $W(\delta q, E)$  along E at these equilibrium locations are extracted and fitted with parabolic functions presented in Equation 12 to obtain the reactant and product Marcus parabolas (see Table 1 and Table 2 for the parameters of Marcus model). These parabolas are distinct with well-separated minimum in the E-space. All three PMFs,

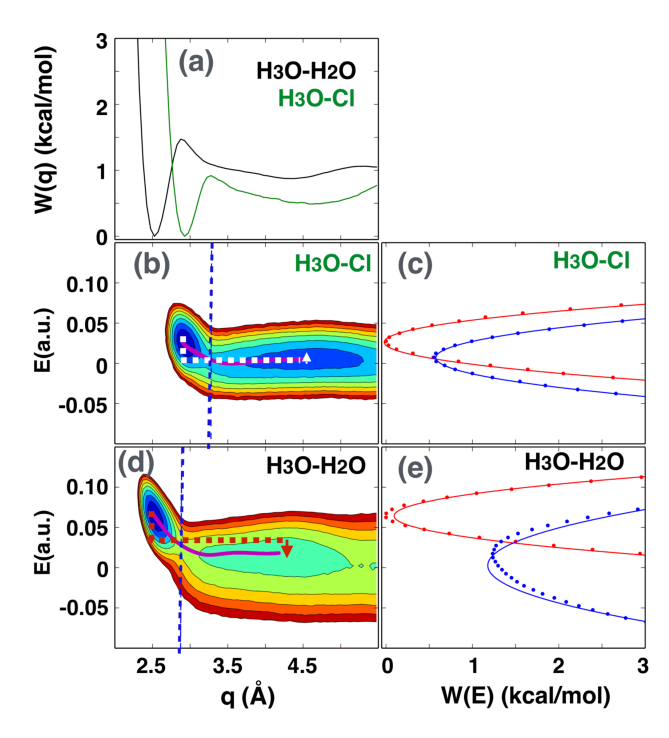


Figure 3: Dissociation of hydronium-water and hydronium-chloride, which describes the vehicular motion of protons, is examined through exploration free energy profiles, W(q), W(q, E), and W(E). Again, Marcus pathways (white, dashed in b and red, dashed in d) follow the minimum free energy pathways (red, solid) in describing these phenomena.In W(q, E), 9 contours are evenly placed between 0 kcal/mol and 3.0 kcal/mol.

namely  $W(\delta q)$ ,  $W(\delta q, E)$ , and W(E), provide the consistent picture of the experiencing a systematic change in electric field from the negative to positive amplitudes going from the hydronium-bound state to neighboring water molecule. Thus, according to Marcus theory presented here, the pathway that describes the reactant-to-product transition involves two steps: First, solvent rearrangement-guided activation in the E-space that leads to the transition state (crossing point between the reactant and product parabolas), and second the transfer of a proton to the neighboring water molecule along  $\delta q$  as the minimum of the product parabola is reached from the transition state.

Analogously, the transfer of a Cl<sup>-</sup> ion from the  $H_3O^+$ -bound state (contact ion-pair state of  $H_3O^+$ -Cl<sup>-</sup>) to the  $H_2O$ -bound (solvent-separated ion-pair state of  $H_3O^+$ -Cl<sup>-</sup>) or breaking of the  $H_3O^+$ -H<sub>2</sub>O hydrogen bond accompanied by water exchange around  $H_3O^+$  follows the same mechanism but with a different electric fields profile (see Figure 3). In the  $H_3O^+$ -bound

Table 1: Parameters for Marcus theory and transmission coefficient and timescale for proton transfer,  $H_3O$ -Cl dissociation, and  $H_3O$ - $H_2O$  dissociation obtained using Marcus theory and TST for the 2M HCl solution.

	Proton transfer	H <sub>3</sub> O-Cl dissociation	H <sub>3</sub> O-H <sub>2</sub> O dissociation
Marcus theory			
$K_{ m R}$	213.093	3625.970	3131.900
$(\text{kcal/mol}/(\frac{E_h/Bohr}{e})^2)$			
$K_{ m P}$	203.664	3175.210	953.597
$(\text{kcal/mol}/(\frac{E_h/Bohr}{e})^2)$			
$\Delta W \; (\text{kcal/mol})$	0.013	-0.009	1.022
$\lambda \; (kcal/mol)$	1.036	0.743	4.912
$\Delta W^{\dagger} + \Delta W_r^{E^{\dagger}}$	0.712	1.225	2.378
(kcal/mol)			
$v_E \left( \frac{E_h/Bohr}{g} f s^{-1} \right)$	0.005	0.001	0.001
C  (kcal/mol)	0.253	0.174	0.799
$\kappa_{ m LZ}$	0.376	0.400	0.944
$\tau = 1/k_{\text{Correct}}^{Marcus} \text{ (ps)}$	1.422	3.776	9.415
TST			
$\kappa_{ m RF}$	0.047	0.070	0.029
$\tau = 1/\kappa_{\rm RF} k_{\rm TST} \ ({\rm ps})$	2.170	3.760	21.61

state, a chloride ion or water molecule experiences a positive electric field that reduces as the chloride ion or a water molecule moves away from the  $H_3O^+$  along larger q direction and fluctuates around a vanishingly small value in the solvent-separated state. Note that, for a given ionic strength of 8M HCl water forms a stronger hydrogen bond with hydronium than the corresponding  $H_3O^+$ -Cl<sup>-</sup> motif. This is indicated by the shorter equilibrium  $H_3O^+$ - $H_2O$  hydrogen-bonding distance than the  $H_3O^+$ -Cl<sup>-</sup>. Interestingly, while the  $H_3O^+$ -Cl<sup>-</sup> interaction strength increases with increasing HCl concentration (the solvent-separated state dominates over the contact ion-pair state at the 2M HCl solution, which is reversed at the 8M HCl solution), the  $H_3O^+$ - $H_2O$  interaction is barely affected (Figure S2 and S3 in the SI) in agreement with a previous study. <sup>31</sup>

Since the Marcus parabolas in Figure 4 cross in the "normal region" for all three cases at 2M HCl concentration and there is a significant gap between the lower and higher energy surfaces (due to strong couplings at the crossing region), they can be treated as

Table 2: Parameters for Marcus theory and transmission coefficient and timescale for proton transfer,  $H_3O$ -Cl dissociation, and  $H_3O$ - $H_2O$  dissociation obtained using Marcus theory and TST for the 8M HCl solution.

	Proton transfer	H <sub>3</sub> O-Cl dissociation	H <sub>3</sub> O-H <sub>2</sub> O dissociation
Marcus theory			
$K_{ m R}$	132.084	2709.340	2437.260
$(\text{kcal/mol}/(\frac{E_h/Bohr}{e})^2)$			
$K_{ m P}$	128.903	2071.410	752.544
$(\text{kcal/mol}/(\frac{E_h/Bohr}{e})^2)$			
$\Delta W \text{ (kcal/mol)}$	0.008	0.598	1.084
$\lambda \; (\text{kcal/mol})$	0.579	0.497	4.627
$\Delta W^{\dagger}$ + $\Delta W_r^{E^{\dagger}}$	0.697	1.232	2.398
(kcal/mol)			
$v_E \left( \frac{E_h/Bohr}{e} fs^{-1} \right)$	0.006	0.001	0.001
C  (kcal/mol)	0.143	0.049	0.751
$\kappa_{ m LZ}$	0.203	0.045	0.945
$\tau = 1/k_{\text{Correct}}^{Marcus} \text{ (ps)}$	2.579	28.923	9.738
TST			
$\kappa_{ m RF}$	0.029	0.033	0.036
$\tau = 1/\kappa_{\rm RF} k_{\rm TST} \ ({\rm ps})$	4.13	12.510	15.250

an adiabatic processes. To further understand the details of proton transfer pathways and the interplay between  $H_3O^+$ - $Cl^-$  dissociation and water exchange around  $H_3O^+$ , we elaborate this adiabatic picture in terms of a set of higher  $(W_+)$  and lower  $(W_-)$  adiabatic surfaces generated through the relation described in the previous section,  $W_{\pm} = \frac{W_R(E) + W_P(E)}{2} \pm \frac{1}{2} \sqrt{4[C(E)]^2 + [W_R(E) - W_P(E)]^2}$ . While the adiabatic picture persists for both proton transfer and water exchange at 8M HCl concentration, the increase in concentration for  $H_3O^+$ - $Cl^-$  dissociation requires a non-adiabatic framework because the diabatic states cross within the "abnormal region" close to the electric field equilibrium in the product state. Thus, the coupling strength between the reactant and product parabolas is very small and accessing to the higher adiabatic free energy surface is necessary to enable the dissociation of the  $H_3O^+$ - $Cl^-$  pair.

Although we have just shown that the Marcus parabolic model can describe different rate processes in the HCl solutions, it of interest to examine whether Marcus pathways outlined

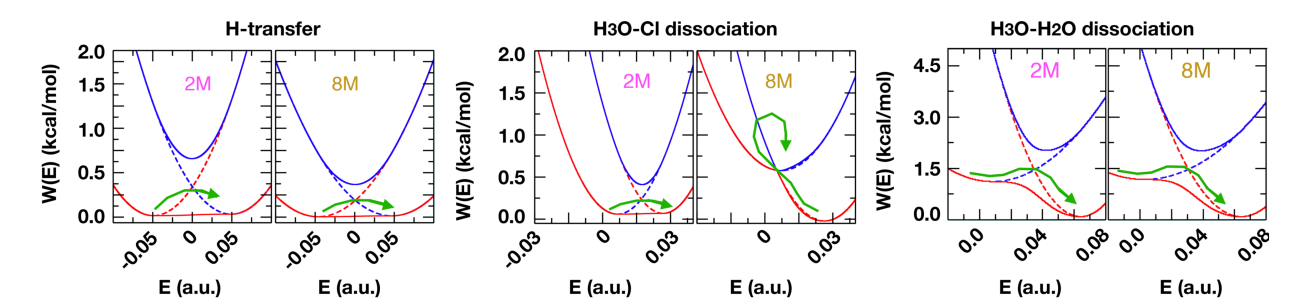


Figure 4: The adiabatic and non-adiabatic picture of different rates processes: The phenomena of proton transfer and hydronium-water and hydronium-chloride dissociation can be explained as the adiabatic traversal of the crossing point of the reactant and product Marcus parabolas, except for the hydronium-chloride dissociation for 8M HCl solution that requires incorporation of the non-adiabatic approach.

above resemble the most probable free-energy pathways between reactant and product basins on the 2D PMF of q and E. To investigate this, we obtain the minimum free energy path (MFEP) as a solution of the dynamical equation in the mass-weighted coordinate system of q and E:

$$\frac{1}{\sqrt{Z}}\frac{d}{ds}\begin{pmatrix} q\\ E \end{pmatrix} = -\sqrt{Z}\begin{pmatrix} \partial_q W\\ \partial_E W \end{pmatrix},\tag{19}$$

where the Z matrix is given by  $Z=\begin{pmatrix} Z_q & Z_{qE} \\ Z_{qE} & Z_E \end{pmatrix}$  and ds is the increment of the path length of the MFEP path vector,  $S=\begin{pmatrix} s_1 \\ s_2 \end{pmatrix}=\frac{1}{\sqrt{Z}}\begin{pmatrix} q \\ E \end{pmatrix}$ . This means,  $ds=\sqrt{(ds_1)^2+(ds_2)^2}$ .

of the MFEP path vector, 
$$S = \begin{pmatrix} s_1 \\ s_2 \end{pmatrix} = \frac{1}{\sqrt{Z}} \begin{pmatrix} q \\ E \end{pmatrix}$$
. This means,  $ds = \sqrt{(ds_1)^2 + (ds_2)^2}$ 

The MFEP is presented along with the Marcus pathway in Figure 2 and Figure 3—their resemblance is excellent. Thus, the construction of a Marcus picture to study both the pathways of rate process of protons in aqueous solutions is consistent with the free-energetically most-likely pathways to the product state. It should be noted that, for obtaining the MFEP, the dependency of  $Z_E$  and  $Z_{qE}$  on the distance coordinate, q, should be considered as they show strong sensitivity to q as presented in Figure S4 in the SI.  $Z_q$  associates with only atomic masses, therefore, it is always constant.

As discussed in the previous section, both Marcus theory and TST must account for

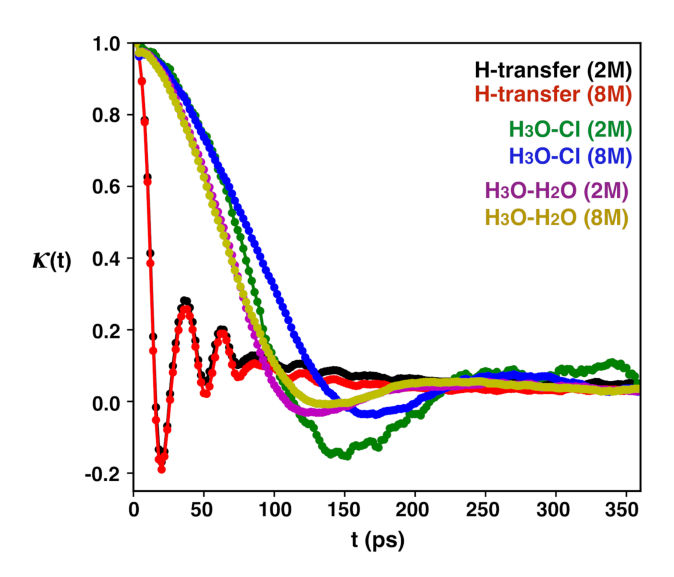


Figure 5: The time-dependent reactive flux transmission coefficient for proton transfer and hydronium-water and hydronium-chloride dissociation, highlighting dynamical stability of protons at the Zundel state indicated by frequent recrossing of this state within the energy diffusion limit.

the non-equilibrium solvent effects through the computation of transmission coefficients to accurately determine the rates of different chemical/physical processes. Herein, we obtained the semiclassical Landau-Zener transmission coefficient ( $\kappa_{\rm LZ}$ ) for Marcus theory and reactive flux transmission coefficient ( $\kappa_{\rm RF}$ ) for TST. While the former is a time-independent quantity as listed in Table 1 and Table 2, the latter decays with time until it reaches to a plateau as depicted in Figure 5. In all cases,  $\kappa_{\rm RF}$  converges to a significantly smaller value than unity as obtained from the plateau and listed in Table 1 and Table 2. This suggests that the distance coordinate suffers from a significant solvent fluctuation-induced barrier-recrossing and provides much slower actual timescales than the TST timescales. It is interesting to see a rapid oscillation of  $\kappa_{\rm RF}$  until 75 ps before  $\kappa_{\rm RF}$  reaches the plateau in the case of proton transfer. Such oscillation also exists for  $\rm H_3O^+$ -Cl $^-$  dissociation and water exchange around  $\rm H_3O^+$ , but it is weak and appears at a later time. This oscillatory behavior is commonly associated with the energy diffusion limit where the thermal energy transfer from the solvent to reaction coordinate is slower.

While  $\kappa_{\rm RF}$  at the plateau region is very similar for all concentrations and all processes,  $\kappa_{\rm LZ}$ 

strongly depends on a specific process because of the distinct coupling between the reactant and product electric field states. For example, at 2M HCl concentration, the coupling is smaller and similar for both proton transfer and  $H_3O^+$ -Cl<sup>-</sup> dissociation leading to smaller  $\kappa_{LZ}$  $(\leq 0.4)$  (Table 1), while for water exchange around  $H_3O^+$  the stronger coupling results in the maximum  $\kappa_{\rm LZ}$  (~ 1). The increase in HCl concentration to 8M reduces  $\kappa_{\rm LZ}$  for proton transfer and H<sub>3</sub>O<sup>+</sup>-Cl<sup>-</sup> dissociation due to the decrease in the reactant-product coupling. However  $\kappa_{\rm LZ}$  does not change for water exchange around  ${\rm H_3O^+}$  as the coupling is not dependent on the ionic strength (Table 1 and Table 2). Regardless of the difference between  $\kappa_{RF}$  and  $\kappa_{LZ}$ , the dynamical separation among proton transfer, H<sub>3</sub>O<sup>+</sup>-Cl<sup>-</sup>, and water exchange around H<sub>3</sub>O<sup>+</sup> is possible to achieve using both the framework of TST and Marcus theory. For 2M HCl concentration, proton transfer between two neighboring water molecules is the fastest process (1-2 ps) and  ${\rm H_3O^+\text{-}Cl^-}$  dissociation is significantly slower ( $\sim 4$  ps). Finally water exchange around  $H_3O^+$  is the slowest process (9-21 ps). Importantly, our study predicts that there is a significant concentration dependency to some of the of the processes discussed herein. 8M HCl leads to two-times slower proton transfer dynamics and four-to-seven times slower H<sub>3</sub>O<sup>+</sup>-Cl<sup>-</sup> dissociation dynamics, interestingly the rate of water exchange around H<sub>3</sub>O<sup>+</sup> is not affected.

Although we are able to examine proton transfer timescales using Marcus theory and TST, the time spent by a proton at the Zundel like transition state cannot be computed by these theories. This is because the Zundel state is not a free energy minimum. However, as indicated by the oscillatory motion of  $\kappa_{RF}(t)$  in Figure 5, the proton exhibits dynamical stability at the Zundel state for a short period of time before it transfers to the neighboring water molecule. The life-time of the Zundel state can then be obtained by determining its time-dependent survival probability,  $(P(t, t + \delta t), t^*)$ . It is assigned to 1 if a proton is located within 0.05 Å of the barrier top of  $W(\delta q)$  in Figure 2 at both times t and  $t + \delta t$  and during the interval of dt it does not leave the neighborhood for any continuous period of time,  $t^*$ . Otherwise,  $P(t, t + \delta t, t^*)$  is set to zero. The life-time of the Zundel state can be determined

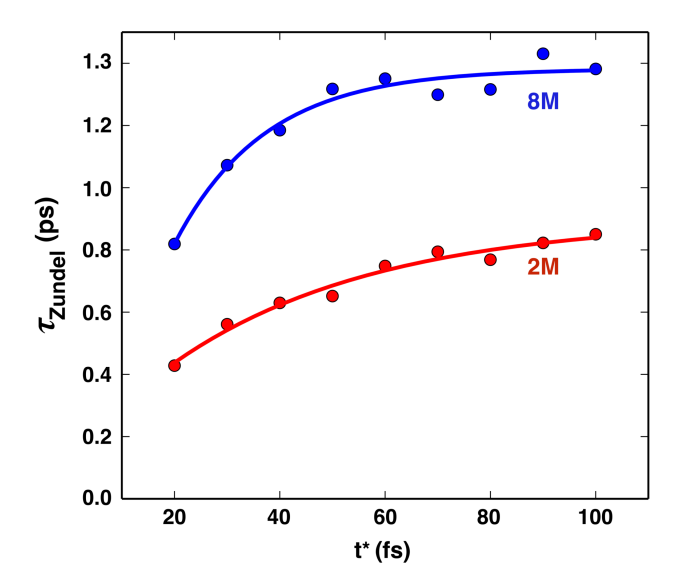


Figure 6: The life-time of the Zundel state as a function of  $t^*$ , indicating a strong dependency on the HCl concentration in aqueous solution.

from the normalized time correlation function of the survival probability:  $^{105}$ 

$$C(t, t^*) = \langle P_i(t, t + \delta t, t^*) \rangle_{i,t} / \langle P(t, t) \rangle_{i,t}.$$
(20)

Here  $\langle ..... \rangle_{i,t}$  represents averaging over all the Zundel states and times. We find  $C(t,t^*)$  to exhibit a bi-exponential behavior depicted in the SI (Figure S5) and show a strong sensitivity to  $t^*$ . The first exponential decay corresponds to a rapid drop of correlation, while the second part indicates a slower decay representing actual departure of the proton from the Zundel state. We have presented the timescales associated with the slower decay in Figure 6, where it is evident that the life-time of a Zundel state increases with increasing  $t^*$  and saturates to some extent between  $t^* = 60$  fs and  $t^* = 100$  fs. Assuming that the maximum allowable value of  $t^*$  is 75 fs, we find that the maximum life-time of the Zundel state is concentration dependent: 800 fs for 2M HCl and 1.25 ps for 8M HCl. Thus, at a given HCl concentration, the life-time of the Zundel state is distinguishable from the dynamics of proton transfer between two neighboring water molecules,  $H_3O^+$ -Cl<sup>-</sup> dissociation, and water exchange around  $H_3O^+$ .

#### **Summary and Conclusion**

Herein, we have provided a detailed molecular picture of proton transfer in aqueous solution using the tools of molecular simulation in conjunction with rate theory. Importantly, this study includes the the effects of ionic strength using interaction potentials based in quantum mechanics (DFT) in addition to treating the nuclei both classically and quantum mechanically. The importance of ionic strength is known to have important consequences providing a novel picture of the correlated local structure of the hydrated proton with the counter-ion in concentrated HCl solutions.<sup>31</sup>

Through the lens of rate theory in the condensed phase we can isolate the important pathways of proton transfer in addition to ion-pair dissociation, and solvent exchange. Interestingly, our study finds that the reaction of proton transfer takes on a concentration dependence that decreases the rate by a factor of 2 from 2M to 8M HCl. Not surprisingly, the processes that takes on the largest concentration dependence is the ion-pairing between H<sub>3</sub>O<sup>+</sup>-Cl<sup>-</sup>, whereas solvent exchange about H<sub>3</sub>O<sup>+</sup> seems to be concentration independent. A theoretical outcome of this study is that, we were able to reproduce the trends in the rates of the aforementioned pathways using both a 2D formulation of TST and a novel formulation of Marcus theory. It is unfortunate, that quantitative agreement was not achieved between the two distinct theoretical approaches. This is most likely due to a couple of factors: First, the one-dimensional formulation of  $\kappa_{RF}$ , that uses only a distance criteria that is known to be an inferior descriptor of rate processes in the condensed phase, and second, the simplification of the prefactor in Marcus rate expression (Equation 15) that will be further examined in the future for obtaining its more accurate description specific to electric field. Nevertheless, the qualitative agreement between TST and Marcus theory are impressive but warrant further investigations to their differences. This will include future exploration of different reaction coordinates (such as the asymmetry coordinate<sup>37</sup>) in addition to different regimes of TST such as the energy diffusion limit.<sup>71</sup>

Last, this study allows us to weigh in on the measurement of the life-time of the Zundel

moiety using 2D IR. 32 Because the Zundel state in our formulation is not a free-energetically stable state (e.g. it is a transition state), we cannot employ the tools of rate theory as defined herein, to predict the life-time of the Zundel state. However, because of the slow thermal energy transfer from the solvent to the proton transfer coordinate, the Zundel state exhibits dynamical stability and we can estimate its life-time by determining its time-dependent survival probability. This analysis reveals that the life-time of the Zundel state is 0.8 ps at 2M and 1.3 ps at 8M, which agrees well with the 2D IR measurements. 32 It should be noted that our AIMD simulations did not consider nuclear quantum effects; if these effects are included in path integral-based AIMD simulations, 106-109 one might find it very challenging to define and distinguish "Eigen"-like and "Zundel"like structures. 36,37,110 Our study demonstrates that the feature of energy diffusion limit, i.e., the slow thermal energy transfer from the solvent to the proton transfer reaction coordinate is imperative to reproduce an accurate experimental estimate of the Zundel life-time. Moreover, we have shown that there is indeed a concentration dependence to the rate of proton transfer which we leave as a prediction for future experimental studies to verify.

### Supporting Information Available

Comparison between the 2DPMFs for 2M HCl and 8M HCl (Figure S1-S3), elements of Z matrix (Figure S4), and survival probability correlation functions (Figure S5).

#### Acknowledgement

S.R., C.J.M., and G.K.S. were supported by the U.S. Department of Energy, Office of Science, Office of Basic Energy Sciences, Division of Chemical Sciences, Geosciences, and Biosciences. M.D.B. was supported by MS<sup>3</sup> (Materials Synthesis and Simulation Across Scales) Initiative, a Laboratory Directed Research and Development Program at Pacific Northwest National

Laboratory (PNNL). T.E.M and J.A.N were supported by the National Science Foundation under Grant No. CHE-1652960. T.E.M also acknowledges support from the Camille Dreyfus Teacher-Scholar Awards Program.

#### References

- Kreuer, K.-D.; Paddison, S. J.; Spohr, E.; Schuster, M. Transport in Proton Conductors for Fuel-Cell Applications: Simulations, Elementary Reactions, and Phenomenology. Chem. Rev. 2004, 104, 4637–4678, PMID: 15669165.
- (2) Winter, M.; Brodd, R. J. What Are Batteries, Fuel Cells, and Supercapacitors? *Chem. Rev.* **2004**, *104*, 4245–4270, PMID: 15669155.
- (3) Heidari, S.; Mohammadi, S. S.; Oberoi, A. S.; Andrews, J. Technical feasibility of a proton battery with an activated carbon electrode. *International Journal of Hydrogen Energy* **2018**, *43*, 6197 6209.
- (4) Colomban, P. Proton conductors and their applications: A tentative historical overview of the early researches. *Solid State Ionics* **2019**, *334*, 125 144.
- (5) Shin, J.-W.; Hammer, N. I.; Diken, E. G.; Johnson, M. A.; Walters, R. S.; Jaeger, T. D.; Duncan, M. A.; Christie, R. A.; Jordan, K. D. Infrared Signature of Structures Associated with the H+(H2O)n (n = 6 to 27) Clusters. Science 2004, 304, 1137–1140.
- (6) Headrick, J. M.; Diken, E. G.; Walters, R. S.; Hammer, N. I.; Christie, R. A.; Cui, J.; Myshakin, E. M.; Duncan, M. A.; Johnson, M. A.; Jordan, K. D. Spectral Signatures of Hydrated Proton Vibrations in Water Clusters. *Science* 2005, 308, 1765–1769.
- (7) Guasco, T. L.; Johnson, M. A.; McCoy, A. B. Unraveling Anharmonic Effects in the

- Vibrational Predissociation Spectra of H5O2+ and Its Deuterated Analogues. *The Journal of Physical Chemistry A* **2011**, *115*, 5847–5858, PMID: 21214227.
- (8) Morrison, A. M.; Flynn, S. D.; Liang, T.; Douberly, G. E. Infrared Spectroscopy of (HCl)m(H2O)n Clusters in Helium Nanodroplets: Definitive Assignments in the HCl Stretch Region. The Journal of Physical Chemistry A 2010, 114, 8090–8098, PMID: 20684581.
- (9) Walewski, L.; Forbert, H.; Marx, D. Quantum Induced Bond Centering in Microsolvated HCl: Solvent Separated versus Contact Ion Pairs. The Journal of Physical Chemistry Letters 2011, 2, 3069–3074.
- (10) Petersen, M. K.; Iyengar, S. S.; Day, T. J. F.; Voth, G. A. The Hydrated Proton at the Water Liquid/Vapor Interface. The Journal of Physical Chemistry B 2004, 108, 14804–14806.
- (11) Mucha, M.; Frigato, T.; Levering, L. M.; Allen, H. C.; Tobias, D. J.; Dang, L. X.; Jungwirth, P. Unified Molecular Picture of the Surfaces of Aqueous Acid, Base, and Salt Solutions. The Journal of Physical Chemistry B 2005, 109, 7617–7623, PMID: 16851882.
- (12) Buch, V.; Milet, A.; Vácha, R.; Jungwirth, P.; Devlin, J. P. Water surface is acidic. Proceedings of the National Academy of Sciences 2007, 104, 7342–7347.
- (13) Iuchi, S.; Chen, H.; Paesani, F.; Voth, G. A. Hydrated Excess Proton at Water Hydrophobic Interfaces. *The Journal of Physical Chemistry B* **2009**, *113*, 4017–4030.
- (14) Jagoda-Cwiklik, B.; Cwiklik, L.; Jungwirth, P. Behavior of the Eigen Form of Hydronium at the Air/Water Interface. The Journal of Physical Chemistry A 2011, 115, 5881–5886, PMID: 21214229.

- (15) Wick, C. D. Hydronium Behavior at the Air-Water Interface with a Polarizable Multistate Empirical Valence Bond Model. The Journal of Physical Chemistry C 2012, 116, 4026–4038.
- (16) Wick, C. D. HCl Accommodation, Dissociation, and Propensity for the Surface of Water. *The Journal of Physical Chemistry A* **2013**, *117*, 12459–12467, PMID: 24168101.
- (17) Baer, M. D.; Kuo, I.-F. W.; Tobias, D. J.; Mundy, C. J. Toward a Unified Picture of the Water Self-Ions at the Air–Water Interface: A Density Functional Theory Perspective. The Journal of Physical Chemistry B 2014, 118, 8364–8372, PMID: 24762096.
- (18) Tse, Y.-L. S.; Chen, C.; Lindberg, G. E.; Kumar, R.; Voth, G. A. Propensity of Hydrated Excess Protons and Hydroxide Anions for the Air-Water Interface. *Journal* of the American Chemical Society 2015, 137, 12610–12616, PMID: 26366480.
- (19) Biswas, R.; Tse, Y.-L. S.; Tokmakoff, A.; Voth, G. A. Role of Presolvation and Anharmonicity in Aqueous Phase Hydrated Proton Solvation and Transport. *The Journal of Physical Chemistry B* 2016, 120, 1793–1804, PMID: 26575795.
- (20) Giberti, F.; Hassanali, A. A. The excess proton at the air-water interface: The role of instantaneous liquid interfaces. *The Journal of Chemical Physics* **2017**, *146*, 244703.
- (21) Das, S.; Imoto, S.; Sun, S.; Nagata, Y.; Backus, E. H. G.; Bonn, M. Nature of Excess Hydrated Proton at the Water-Air Interface. *Journal of the American Chemical Society* **2020**, *142*, 945–952, PMID: 31867949.
- (22) Petersen, P. B.; Saykally, R. J. Evidence for an Enhanced Hydronium Concentration at the Liquid Water Surface. The Journal of Physical Chemistry B 2005, 109, 7976– 7980, PMID: 16851932.
- (23) Levering, L. M.; Sierra-Hernandez, M. R.; Allen, H. C. Observation of Hydronium

- Ions at the Air Aqueous Acid Interface: Vibrational Spectroscopic Studies of Aqueous HCl, HBr, and HI. *The Journal of Physical Chemistry C* **2007**, *111*, 8814–8826.
- (24) Tian, C.; Ji, N.; Waychunas, G. A.; Shen, Y. R. Interfacial Structures of Acidic and Basic Aqueous Solutions. *Journal of the American Chemical Society* 2008, 130, 13033– 13039, PMID: 18774819.
- (25) Baer, M. D.; Tobias, D. J.; Mundy, C. J. Investigation of Interfacial and Bulk Dissociation of HBr, HCl, and HNO3 Using Density Functional Theory-Based Molecular Dynamics Simulations. The Journal of Physical Chemistry C 2014, 118, 29412–29420.
- (26) Das, S.; Bonn, M.; Backus, E. H. G. The Surface Activity of the Hydrated Proton Is Substantially Higher than That of the Hydroxide Ion. *Angewandte Chemie International Edition* **2019**, *58*, 15636–15639.
- (27) Weissenborn, P. K.; Pugh, R. J. Surface Tension of Aqueous Solutions of Electrolytes: Relationship with Ion Hydration, Oxygen Solubility, and Bubble Coalescence. *Journal of Colloid and Interface Science* **1996**, 184, 550 – 563.
- (28) Pegram, L. M.; Record, M. T. Partitioning of atmospherically relevant ions between bulk water and the water/vapor interface. *Proceedings of the National Academy of Sciences* **2006**, *103*, 14278–14281.
- (29) Lewis, T.; Winter, B.; Stern, A. C.; Baer, M. D.; Mundy, C. J.; Tobias, D. J.; Hemminger, J. C. Dissociation of Strong Acid Revisited: X-ray Photoelectron Spectroscopy and Molecular Dynamics Simulations of HNO3 in Water. The Journal of Physical Chemistry B 2011, 115, 9445–9451, PMID: 21688845.
- (30) Lewis, T.; Winter, B.; Stern, A. C.; Baer, M. D.; Mundy, C. J.; Tobias, D. J.; Hemminger, J. C. Does Nitric Acid Dissociate at the Aqueous Solution Surface? The Journal of Physical Chemistry C 2011, 115, 21183–21190.

- (31) Baer, M. D.; Fulton, J. L.; Balasubramanian, M.; Schenter, G. K.; Mundy, C. J. Persistent Ion Pairing in Aqueous Hydrochloric Acid. *The Journal of Physical Chemistry B* **2014**, *118*, 7211–7220, PMID: 24837190.
- (32) Thämer, M.; De Marco, L.; Ramasesha, K.; Mandal, A.; Tokmakoff, A. Ultrafast 2D IR spectroscopy of the excess proton in liquid water. *Science* **2015**, *350*, 78–82.
- (33) Lewis, N. H. C.; Fournier, J. A.; Carpenter, W. B.; Tokmakoff, A. Direct Observation of Ion Pairing in Aqueous Nitric Acid Using 2D Infrared Spectroscopy. *The Journal of Physical Chemistry B* **2019**, *123*, 225–238.
- (34) dos Santos, A. P.; Levin, Y. Surface tensions and surface potentials of acid solutions.

  The Journal of Chemical Physics 2010, 133, 154107.
- (35) Duignan, T. T.; Parsons, D. F.; Ninham, B. W. Hydronium and hydroxide at the air-water interface with a continuum solvent model. *Chemical Physics Letters* 2015, 635, 1 – 12.
- (36) Daly, C. A.; Streacker, L. M.; Sun, Y.; Pattenaude, S. R.; Hassanali, A. A.; Petersen, P. B.; Corcelli, S. A.; Ben-Amotz, D. Decomposition of the Experimental Raman and Infrared Spectra of Acidic Water into Proton, Special Pair, and Counterion Contributions. The Journal of Physical Chemistry Letters 2017, 8, 5246–5252, PMID: 28976760.
- (37) Napoli, J. A.; Marsalek, O.; Markland, T. E. Decoding the spectroscopic features and time scales of aqueous proton defects. *The Journal of chemical physics* **2018**, *148*, 222833.
- (38) Yuan, R.; Napoli, J. A.; Yan, C.; Marsalek, O.; Markland, T. E.; Fayer, M. D. Tracking Aqueous Proton Transfer by Two-Dimensional Infrared Spectroscopy and ab Initio Molecular Dynamics Simulations. ACS Central Science 2019, 5, 1269–1277.

- (39) Peters, B. Reaction rate theory and rare events; Elsevier Science: Oxford, 2016.
- (40) Pollak, E.; Talkner, P. Reaction Rate Theory: What It Was, Where Is It Today, and Where Is It Going? *CHAOS* **2005**, *15*, 026116.
- (41) Eyring, H. The theory of absolute reaction rates. Trans. Faraday Soc. 1938, 34, 41–48.
- (42) Wigner, E. The transition state method. Trans. Faraday Soc. 1938, 34, 29-41.
- (43) Schenter, G.; Garrett, B. C.; Truhlar, D. G. Generalized transition state theory in terms of the potential of mean force. *J. Chem. Phys.* **2003**, *119*, 5828–5833.
- (44) Truhlar, D. G.; Garrett, B. C. Variational transition state theory. Ann. Rev. Phys. Chem. 1984, 35, 159–189.
- (45) Kramers, H. Brownian motion in a field of force and the diffusion model of chemical reactions. *Physica* **1940**, *7*, 284–304.
- (46) Pollak, E. Theory of activated rate processes: A new derivation of Kramers' expression.

  J. Chem. Phys. 1986, 85, 865.
- (47) Grote, R. F.; Hynes, J. T. The stable states picture of chemical reactions. II. Rate constants for condensed and gas phase reaction models. *J. Chem. Phys.* **1980**, *73*, 2715.
- (48) Bennett, C. H. Algorithms for chemical computations, ACS symposium series; American Chemical Society: Washington, D.C., USA, 1977.
- (49) Chandler, D. Statistical mechanics of isomerization dynamics in liquids and the transition state approximation. *J. Chem. Phys.* **1978**, *68*, 2959–2970.
- (50) Truhlar, D. G.; Garrett, B. C.; Klippenstein, S. J. Current Status of Transition-State Theory. J. Phys. Chem. 1996, 100, 12771.

- (51) Guàrdia, E.; Rey, R.; Padró, J. A. Potential of mean force by constraint molecular dynamics: A sodium chloride ion-pair in water. *Chem. Phys.* **1991**, *155*, 187–195.
- (52) Dellago, C.; Bolhuis, P. G.; Geissler, P. L. Transition path sampling. *Advances in Chemical Physics* **2002**, *123*, 1.
- (53) Mullen, R. G.; Shea, J. E.; Peters, B. Transmission Coefficients, Committors, and Solvent Coordinates in Ion-Pair Dissociation. J. Chem. Theory Comput. 2014, 10, 659.
- (54) Annapureddy, H. V. R.; Dang, L. X. Understanding the Rates and Molecular Mechanism of Water Exchange Around Aqueous Ions Using Molecular Simulations. J. Phys. Chem. B 2014, 118, 8917.
- (55) Annapureddy, H. V. R.; Dang, L. X. Water exchange rates and molecular mechanism around aqueous halide ions. *J. Phys. Chem. B* **2014**, *118*, 7886.
- (56) Dang, L. X.; Annapureddy, H. V. R. Computational studies of water exchange around aqueous Li<sup>+</sup> with polarizable potential models. *J. Chem. Phys.* **2013**, *139*, 084506.
- (57) Hermansson, K.; Wojcik, M. Water exchange around Li<sup>+</sup> and Na<sup>+</sup> in LiCl (aq) and NaCl (aq) from MD Simulations. J. Phys. Chem. B **1998**, 102, 6089.
- (58) Wilkins, D. M.; Manolopoulos, D. E.; Dang, L. X. Nuclear quantum effects in water exchange around lithium and fluoride ions. *J. Chem. Phys.* **2015**, *142*, 064509.
- (59) Roy, S.; Dang, L. X. Water exchange dynamics around  $H_3O^+$  and  $OH^-$  ions. Chem. Phys. Lett. **2015**, 628, 30–34.
- (60) Rey, R.; Hynes, J. T. Hydration shell exchange dynamics for Na<sup>+</sup> in water. *J. Phys.:*Condens. Matter **1996**, 8, 9411.

- (61) Spangberg, D.; Wojcik, M.; Hermansson, K. Pressure dependence and activation volume for the water exchange mechanism in NaCl (aq) from MD simulations. Chem. Phys. Lett. 1997, 276, 114.
- (62) Dang, L. X. Computational studies of water-exchange rates around aqueous Mg<sup>2+</sup> and Be<sup>2+</sup>. J. Phys. Chem. C **2014**, 118, 29028.
- (63) Roy, S.; Dang, L. X. Computer simulation of methanol exchange dynamics around cations and anions. *J. Phys. Chem. B* **2016**, *120*, 1440–1445.
- (64) Danga, L. X.; Vob, Q. N.; Nilssonb, M.; Nguyenb, H. D. Rate theory on water exchange in aqueous uranyl ion. *Chem. Phys. Lett.* **2017**, *671*, 58.
- (65) Pluhařová, E.; Baer, M. D.; Schenter, G. K.; Jungwirth, P.; Mundy, C. J. Dependence of The Rate of LiF Ion-Pairing on The Description of Molecular Interaction. J. Phys. Chem. B 2016, 120, 1749.
- (66) Truhlar, D. Variational transition state theory and multidimensional tunneling for simple and complex reactions in the gas phase, solids, liquids, and enzymes; in Isotope effects in chemistry and biology, Marcel Dekker Inc, New York, 2006; pp 579–619.
- (67) Peters, B. Inertial likelihood maximization for reaction coordinates with high transmission coefficients. *Chem. Phys. Lett.* **2012**, *554*, 248–253.
- (68) Roy, S.; Baer, M. D.; Mundy, C. J.; Schenter, G. K. Marcus theory of ion-pairing. *J. Chem. Theory Comput.* **2017**, *13*, 3470–3477.
- (69) Roy, S.; Galib, M.; Schenter, G. K.; Mundy, C. J. On the relation between Marcus theory and ultrafast spectroscopy of solvation kinetics. *Chem. Phys. Lett.* **2018**, *692*, 407–415.
- (70) Roy, S.; Bryantsev, V. S. Finding Order in the Disordered Hydration Shell of Rapidly

- Exchanging Water Molecules around the Heaviest Alkali Cs<sup>+</sup> and Fr<sup>+</sup>. J. Phys. Chem. B **2018**, 122, 12067–12076.
- (71) Reese, S. K.; Tucker, S. C.; Schenter, G. K. The reactive flux method in the energy diffusion regime. II. Importance of the solvent's spectral profile. J. Chem. Phys. 1995, 102, 104–118.
- (72) Roy, S.; Lessing, J.; Meisl, G.; Ganim, Z.; Tokmakoff, A.; Knoester, J.; Jansen, T. L. C. Solvent and conformation dependence of amide I vibrations in peptides and proteins containing proline. J. Chem. Phys. 2011, 135, 234507–234507.
- (73) Wang, L.; Middleton, C. T.; Zanni, M. T.; Skinner, J. L. Development and validation of transferable amide I vibrational frequency maps for peptides. *J. Phys. Chem. B* **2011**, *115*, 3713–3724.
- (74) Gruenbaum, S. M.; Tainter, C. J.; Shi, L.; Ni, Y.; Skinner, J. L. Robustness of frequency, transition dipole, and coupling maps for water vibrational spectroscopy. J. Chem. Th. Comp. 2013, 9, 3109–3117.
- (75) Darve, E.; Pohorille, A. Calculating free energies using average force. *J. Chem. Phys.* **2001**, *115*, 9169–9183.
- (76) Dang, L. X.; Chang, T.-M. Molecular dynamics study of water clusters, liquids, and liquid-vapor interface of water with many-body potentials. J. Chem. Phys. 1997, 106, 8149.
- (77) Roy, S.; Baer, M. D.; Mundy, C. J.; Schenter, G. K. Reaction rate theory in coordination number space: An application to ion solvation. J. Chem. Phys. C 2016, 120, 7597–7605.
- (78) Schenter, G. K.; Garrett, B. C.; Truhlar, D. G. The Role of Collective Solvent Coor-

- dinates and Nonequilibrium Solvation in Charge-Transfer Reactions. *J. Chem. Phys.* B **2001**, *105*, 9672.
- (79) Landau, L. D. A theory of energy transfer on collisions. *Physik. Z. Sowjet.* **1932**, *1*, 88.
- (80) Landau, L. D. A theory of energy transfer II. Physik. Z. Sowjet. 1932, 2, 46.
- (81) Zener, C. Non-adiabatic crossing of energy levels. *Proc. R. Soc. London* **1932**, *137*, 696–702.
- (82) Newton, M. D.; Sutin, N. Electron transfer reactions in condensed phases. *Ann. Rev. Phys. Chem.* **1984**, *35*, 437–480.
- (83) Green, D.; Perry, R. Perry's Chemical Engineers' Handbook, Eighth Edition (Chemical Engineers Handbook); McGraw-Hill Education, 2007.
- (84) Ceriotti, M.; More, J.; Manolopoulos, D. E. i-PI: A Python interface for ab initio path integral molecular dynamics simulations. Computer Physics Communications 2013, 185, 1019–1026.
- (85) Kapil, V.; Rossi, M.; Marsalek, O.; Petraglia, R.; Litman, Y.; Spura, T.; Cheng, B.; Cuzzocrea, A.; Meißner, R. H.; Wilkins, D. M., et al. i-PI 2.0: A universal force engine for advanced molecular simulations. Computer Physics Communications 2019, 236, 214–223.
- (86) Tuckerman, M.; Berne, B. J.; Martyna, G. J. Reversible multiple time scale molecular dynamics. *The Journal of Chemical Physics* **1992**, *97*, 1990.
- (87) Bussi, G.; Donadio, D.; Parrinello, M. Canonical sampling through velocity rescaling.

  The Journal of chemical physics 2007, 126, 014101.

- (88) Ceriotti, M.; Parrinello, M.; Markland, T. E.; Manolopoulos, D. E. Efficient stochastic thermostatting of path integral molecular dynamics. *The Journal of chemical physics* **2010**, *133*, 124104.
- (89) VandeVondele, J.; Krack, M.; Mohamed, F.; Parrinello, M.; Chassaing, T.; Hutter, J. Quickstep: Fast and accurate density functional calculations using a mixed Gaussian and plane waves approach. *Computer Physics Communications* **2005**, *167*, 103–128.
- (90) Hutter, J.; Iannuzzi, M.; Schiffmann, F.; VandeVondele, J. CP2K: Atomistic simulations of condensed matter systems. Wiley Interdisciplinary Reviews: Computational Molecular Science 2014, 4, 15–25.
- (91) Perdew, J. P.; Burke, K.; Ernzerhof, M. Generalized Gradient Approximation Made Simple. *Physical Review Letters* **1996**, *77*, 3865–3868.
- (92) Zhang, Y.; Yang, W. Comment on "Generalized Gradient Approximation Made Simple". *Physical Review Letters* **1998**, *80*, 890–890.
- (93) Grimme, S.; Antony, J.; Ehrlich, S.; Krieg, H. A consistent and accurate ab initio parametrization of density functional dispersion correction (DFT-D) for the 94 elements H-Pu. *The Journal of chemical physics* **2010**, *132*, 154104.
- (94) Goedecker, S.; Teter, M.; Hutter, J. Separable dual-space Gaussian pseudopotentials. *Physical Review B* **1996**, *54*, 1703–1710.
- (95) Lippert, G.; Hutter, J.; Parrinello, M. A hybrid Gaussian and plane wave density functional scheme. *Molecular Physics* **1997**, *92*, 477–488.
- (96) VandeVondele, J.; Hutter, J. An efficient orbital transformation method for electronic structure calculations. *The Journal of Chemical Physics* **2003**, *118*, 4365.
- (97) Kolafa, J. Time-reversible always stable predictor-corrector method for molecular dynamics of polarizable molecules. *Journal of computational chemistry* **2004**, *25*, 335–42.

- (98) Kühne, T.; Krack, M.; Mohamed, F.; Parrinello, M. Efficient and Accurate Car-Parrinello-like Approach to Born-Oppenheimer Molecular Dynamics. *Physical Review Letters* **2007**, *98*, 1–4.
- (99) Gaus, M.; Cui, Q.; Elstner, M. DFTB3: Extension of the self-consistent-charge density-functional tight-binding method (SCC-DFTB). Journal of Chemical Theory and Computation 2011, 7, 931–948.
- (100) Aradi, B.; Hourahine, B.; Frauenheim, T. DFTB+, a sparse matrix-based implementation of the DFTB method. *Journal of Physical Chemistry A* **2007**, *111*, 5678–5684.
- (101) Gaus, M.; Goez, A.; Elstner, M. Parametrization and benchmark of DFTB3 for organic molecules. *Journal of Chemical Theory and Computation* **2013**, *9*, 338–354.
- (102) Jahangiri, S.; Dolgonos, G.; Frauenheim, T.; Peslherbe, G. H. Parameterization of halogens for the density-functional tight-binding description of halide hydration. *Jour*nal of Chemical Theory and Computation 2013, 9, 3321–3332.
- (103) Zhechkov, L.; Heine, T.; Patchkovskii, S.; Seifert, G.; Duarte, H. A. An efficient a posteriori treatment for dispersion interaction in density-functional-based tight binding. *Journal of Chemical Theory and Computation* 2005, 1, 841–847.
- (104) Rappé, A.; Casewit, C. J.; Colwell, K. S.; Goddard III, W. A.; Skiff, W. M. UFF, a Full Periodic Table Force Field for Molecular Mechanics and Molecular Dynamics Simulations. J. Am. Chem. Soc. 1992, 114, 10024–10035.
- (105) Impey, R. W.; Madden, P. A.; Mcdonald, I. R. Hydration and mobility of ions in solution. J. Phys. Chem. 1983, 87, 5071–5083.
- (106) Habershon, S.; Manolopoulos, D. E.; Markland, T. E.; III, T. F. M. Ring-polymer molecular dynamics: quantum effects in chemical dynamics from classical trajectories in an extended phase space. Annu. Rev. Phys. Chem. 2013, 64, 387.

- (107) Craig, I. R.; Manolopoulos, D. E. Quantum statistics and classical mechanics: Real time correlation functions from ring polymer molecular dynamics. J. Chem. Phys. 2004, 121, 3368.
- (108) Cao, J.; Voth, G. A. The formulation of quantum statistical mechanics on the Feynman path centroid density .IV. Algorithm for centroid molecular dynamics. *J. Chem. Phys.* **1994**, *101*, 6168.
- (109) Jang, S.; Voth, G. A. A derivation of centroid molecular dynamics and other approximate time evolution methods for path integral centroid variables. *The Journal of Chemical Physics* **1999**, *111*, 2371–2384.
- (110) Marx, D.; Tuckerman, M. E.; Parrinello, M. Solvated excess protons in water: quantum effects on the hydration structure. *Journal of Physics: Condensed Matter* 2000, 12, A153–A159.

## TOC Graphic

